3C-3D VSP: The Blackfoot experiment

Jitendra S. Gulati, Robert R. Stewart, and John M. Parkin*

ABSTRACT

A 3C-3D VSP was acquired over the Blackfoot oil field in Alberta, Canada in 1995. The 3-D VSP was recorded simultaneously with a surface 3C-3D seismic program. The objectives of the 3-D VSP were to define recording logistics, develop data handling and processing procedures, and determine if the 3-D VSP could image the reservoir.

The shots in the surface 3C-3D seismic survey that fell within 2200m offset from the recording well were used in the 3-D VSP. As the shots for the surface 3-D were being taken, the borehole tool moved seven times (75m each) recording over a receiver depth range from 400m to 910m. The 3-D VSP data were processed using basic VSP processing techniques that involved hodogram analysis, wavefield separation using median filters, and VSP deconvolution. The P-P and P-S volumes from the 3-D VSP were then obtained by VSPCDP stacking the upgoing wavefields in 3-D cells followed by f-xy deconvolution. Final P-P and P-S images from the 3-D VSP correlate well with those from the surface 3C-3D survey. Time slices from the 3-D VSP also indicate the trend of the Glauconitic sand channel of the Blackfoot field.

INTRODUCTION

From Stewart and Gulati (1997), we know that borehole seismic surveys have a long history of providing rock properties such as interval velocity, impedance and attenuation near the borehole. These surveys have also assisted surface-seismic interpretation through time-to-depth values and the provision of a zero-phase reflectivity that is largely multiple-free. These results are basically one-dimensional within a Fresnel zone near the borehole.

With the advent of offset source positions, techniques were developed to obtain a structural image from VSP data (Wyatt and Wyatt, 1984; Chang and McMechan, 1986, Whitmore and Lines, 1986). These produced credible 2-D sections. While valuable, this 2-D VSP image still had limitations such as suffering from restricted angular coverage per bin, limited total bin fold, and difficulty tying various shot statics and moveout.

The fundamental 2-D limitation in the VSP, and indeed many of the other previously mentioned problems, can be overcome by using an areal distribution of shot points, or in the reverse VSP case an areal distribution of receivers. This allows a 3-D image to be constructed near the borehole.

Interest in 3-D well seismic data led to investigations of the feasibility and advantages of using the 3-D VSP geometry. Chen and McMechan (1992) used a pre-

* Baker Atlas, Calgary

Contents

stack depth migration algorithm and synthetic 3-D reverse VSP data to investigate imaging of salt structures. They found that 3-D imaging provided imaging of dips and structures not normally accessible to surface surveys. Sun and Stewart (1994) used raytracing over a dome model in a synthetic 3-D reverse VSP and found that converted-waves provided significant coverage of the dome compared to compressional waves. Clochard et al. (1997) used pre-stack migrations and showed the ability of 3-D VSP to image complex structures.

Early 3-D VSP surveys included those conducted by AGIP in 1986 in Brenda field and the 1989 Ekofisk 3-D VSP by Phillips Petroleum group of companies (Dangerfield, 1996). Subsequent to these, several more 3-D VSPs have been shot. Shekhtman et al. (1993) outlined a land VSP where they used vibrators over an area and a 3-level VSP tool to construct a 3-D image. Shell, UK shot a 3-D VSP over the Brent field, North Sea in 1993 for optimizing the development of the field (Van der Pal et al., 1996). The Ekofisk reservoir was revisited and more 3-D VSPs were shot over the field (Farmer et al., 1997; Omnes and Clough, 1998). Fairborn and Harding, Jr. (1996) showed a case in Louisiana of using a downhole vibratory source and a surface spread of receivers to reconstruct a 3-D tomographic image of a sinkhole. A CREWES-supported group shot a 3-D VSP over the Blackfoot field in 1995 simultaneously with a surface 3C-3D survey. The main goal was to assess the 3-D VSP capability for improved delineation of a Glauconitic sand-channel (Stewart and Zhang, 1996). Recently, a 3-D VSP was shot over BP's Magnus field to improve structural interpretation of the field (First Break, 1997).

Several authors have analysed 3-D VSP data processing. Sun and Stewart (1994) proposed a processing flow that included common receiver and common shot gathering, statics removal, binning, and pre-stack migration. Boelle et al. (1998) describe the whole processing sequence used for processing the Oseberg 3-D VSP data. Zhang et al. (1997) developed rapid moveout correction and VSPCDP mapping methods to process the Blackfoot 3-D VSP survey. Chen (1998), and Chen and Peron (1998) implemented the ray-trace mapping method using 3-D velocity models and applied it to real data. Farmer et al. (1997) used a 3-D tomographic inversion scheme for determining velocities in the depth migration of a 3-D VSP survey over the Ekofisk field. Mittet et al. (1997) used a 3-D elastic reverse time migration scheme and applied it to synthetic and the Oseberg 3C-3D VSP circular shoot. Clochard et al. (1998) showed that elastic depth migration of the Oseberg VSP data with no wavefield separation gave interpretable images consistent with those obtained after wavefield separation. Bicquart (1998) applied Kirchhoff depth migration to two real data examples and obtained images comparable with those from surface 3-D seismic.

Standard 3-D seismic interpretive techniques have also been applied to the 3-D volume obtained from the 3-D VSP surveys. The 1989 Ekofisk 3-D VSP resulted in a clear image where the surface 3-D had failed (Dangerfield, 1996). The Brent 3-D VSP revealed fault patterns that were more complex and resolved compared to those from the surface seismic (Van der Pal et al., 1996). Results from an initial 3-D VSP processing flow over the Blackfoot field resulted in an image consistent with that of a 3-D surface seismic survey in the area (Zhang et al., 1997). Farmer et al. (1997) indicate that processing of a later 3-D VSP survey over the Ekofisk field resulted in a vastly improved image of the Ekofisk reservoir. Boelle et al. (1998) observed that the

3-D borehole seismic gave more details within the reservoir formation compared to the surface seismic. These results show the promise of the 3-D VSP and are nicely summarized by Dangerfield's (1996) statement:

> *"3-D borehole profiles should be considered as a working alternative to 2-D borehole profiles since the extra rig time and cost are surprisingly small and the benefits of 3-D are substantial".*

In this paper, results from the Blackfoot 3C-3D VSP are presented. Initial results from the Blackfoot survey were first presented by Zhang et al. (1997). Since then developments in the processing flow have resulted in an improved image of the channel body in the area and new results presented in this chapter. The following sections give details of the survey from the acquisition to the interpretation stage.

ACQUISITION OF THE BLACKFOOT 3C-3D VSP

In 1995, a 3C-3D VSP survey was conducted by a CREWES-supported group by recording an existing 3C-3D surface survey over the Blackfoot field. The Blackfoot field, which is owned by PanCanadian Petroleum Ltd., is located about 15 kilometres southeast of Strathmore in Alberta, Canada. The producing formation within the Blackfoot area is a Lower Cretaceous, cemented glauconitic sand. The sand was deposited as incised channel-fill sediments above Mississippian carbonates (Wood and Hopkins, 1992). The glauconitic sandstone lies at a depth of about 1,500m below surface and is up to 45m thick. The average porosity in this producing sandstone is near 18% and the cumulative production from it throughout southern Alberta exceeds 200 million barrels of oil and 400 BCF gas (Margrave et al., 1998).

The simultaneous monitoring of shots used in the surface 3C-3D program enabled very cost-effective acquisition of the 3-D VSP survey. The objectives of the survey were (i) to see if it was logistically possible, (ii) to develop acquisition and processing procedures for 3-D VSP, and (iii) to determine if the 3-D VSP data could better image the channel body.

The downhole recording of the surface shots was acquired in well 12-16 (Figure 1) using Baker Atlas's 5-level receiver tool. The 3-D VSP recorded 431 source locations, 4 kg. of dynamite in 18 m holes arranged in 12 lines. The 12 north-south shot lines for the 3-D VSP were spaced 210 m apart with a shot interval of 60 m. Only the shots within 2200 m offset from the well were used out of the total 1395 sources acquired in the whole 3C-3D survey. The shot parameters were designed to meet the criteria of the surface survey and were not optimized for the 3-D VSP survey.

Zhang et al. (1997) indicate that it was intended to have the receiver tool deep in the well for near-offset shots to obtain high-resolution coverage of the target near the borehole and good velocity control. The tool would then be moved progressively shallower for far-offset shots to obtain wider sub-surface coverage. However, field logistics dictated otherwise as the surface shooting used four shooters at variable locations, who fired when ready. It was then decided in the field that the downhole tool would record a minimum of 40 shots before moving to the next interval

regardless of source locations. This minimized the number of downhole receiver moves and thus missed shots. Over the course of the survey, the receiver tool was moved seven times (75 m each) to give a receiver depth range from 400m to 910m.

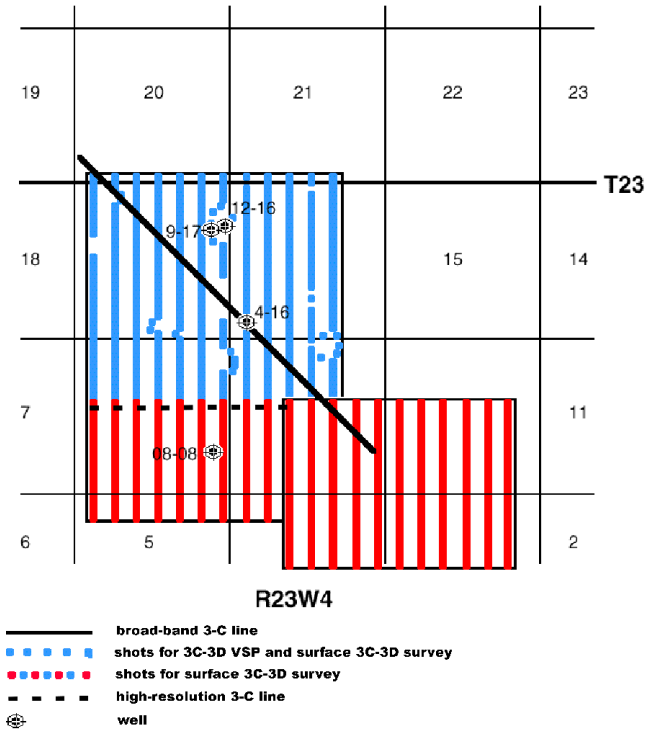

Fig.1. Map of the Blackfoot surveys showing shot points for the surface 3C-3D and the 3C-3D VSP. A previous broad-band and a recent high-resolution 3-C line are also shown in the figure (modified from Zhang et al., 1996).

PROCESSING THE 3C-3D VSP DATA

Initial analysis and processing of the raw data was first performed by Zhang et al. (1996). The results from an improved processing flow are presented here. The first objective of processing the data was to separate the upgoing compressional and shear wavefields. This was followed by mapping of the upgoing P-waves and converted-waves to obtain 3-D images from the survey.

Upgoing compressional and shear wavefield separation

The data were processed by Baker Atlas to obtain the upgoing compressional and shear wavefields. Although the data volume for the entire 3-D VSP survey was small (about 2000 traces per component), processing the data with conventional VSP wavefield separation techniques posed new challenges. Wavefield separation and VSP deconvolution had to be applied with care in lieu of having only 5 levels of receivers for each shot. Figure 2 outlines the steps followed by Bkaer Atlas in processing the raw data to separate the two upgoing wavefields and is discussed in the following sections.

Figures 3a-3c show the raw shot gathers for shot at an offset of 372m from the well. Apart from the direct arrivals, it is very difficult to see any events on these gathers. The coupling resonance is seen to be stronger on the two horizontal components compared to the vertical component. This indicates that the VSP sonde carrying the three-component geophones is well coupled vertically but not horizontally for the receiver depths shown in the figures.

After geometry and trace edits, shot statics from the surface 3-D survey were applied to the three-component VSP data. This was followed by hodogram analysis of the two horizontal components (here referred to as H1 and H2) in a small window around the direct arrivals. Hodogram analysis was used to align one of the horizontal components in the direction of the source. The horizontal component aligned in the direction of the source is henceforth referred to as the radial component and the other as the transverse component. Figure 3d is the radial component data obtained after hodogram analysis of the H1 and H2 shots gathers of Figures 3b and 3c respectively. It is interesting to note that the presence of casing resonance is weaker on 910m receiver on the radial component than on the corresponding H2 component. A downgoing wave at about 880ms is also decipherable on the radial component.

The same exponential gain correction was applied to both the vertical and radial component data. The two datasets were time-shifted using first-break arrival times to align downgoing P-waves on both of them. A small median filter of seven traces was then used to separate downgoing P-waves from the data. Next, downgoing converted-waves were separated from the data by using a median filter based on the moveout of the downgoing converted-wave. Figures 3e-3f show the resultant downgoing and upgoing compressional and shear wavefields. Although downgoing and upgoing events are now visible, wavefield separation has also resulted in upgoing energy leaking onto the downgoing part of the wavefield. Nonetheless, the results are satisfactory considering that there were only five receiver depths for each shot location. Use of a modal filter (Esmersoy, 1990; Labonte, 1990) would probably give better results than those shown in Figure 3.

Upgoing converted-waves and P-waves were then removed from the vertical and radial component data respectively by using a three-trace median filter based on the moveout of the downgoing P-waves. This was followed by a trace-by-trace VSP deconvolution (Kennett et al., 1980) based on the downgoing P-waves in a window of 180ms around the first-breaks to give the P-wave and converted-wave reflectivity traces (Figure 4).

From the shot gathers in Figure 4, we observe that data on the radial component has larger moveout compared to that on the vertical component data, thereby, indicating effective wavefield separation. The process of obtaining upgoing P-wave and converted-wave reflections was carried out either on a trace-by-trace basis or in shot gathers. So in this context, it is important to verify the results by making some observations on receiver gathers of the data (Figures 5-7). As the data on each component is a superposition of several wavefields, the receiver gathers in general look noisy. Nonetheless, several events can be seen on both the raw vertical component and one of the horizontal components of the data (Figures 5 and 6). The H2 horizontal component (Figure 7) appears to be mainly dominated by noise. The

upgoing deconvolved P-wave and converted-wave reflections are shown in Figures 8 and 9 respectively. The reflection signals are stronger on both the vertical and radial component receiver gathers. The results of processing the data are more evident on the radial component data. In Figures 6 and 7, the raw horizontal components lack regular moveout of events. On the contrary, the radial component in Figure 9 shows regular moveout of events. Also, events on the radial component data have larger moveout with offsets when compared to the vertical component data. These observations increase confidence about the processing results.

P-wave and converted-wave 3-D imaging

The deconvolved upgoing P-wave and converted-wave reflections were then used to generate 3-D volumes. The fold distribution for the P-wave at the target depth of 1500m was calculated for different bin configurations using a straight-ray approximation. A bin size of 110m by 20m was then decided upon as the smallest bin size that gave uniform fold distribution at the target depth (Figure 11). Due to the sparse data of about 2000 traces and reflection coverage of about a square km. at the target depth, the average fold per bin location was a small number. Moreover, although the bin size of 110m by 20m resulted in uniform fold distribution, the azimuth and offset coverage in each bin was somewhat variable. This was unavoidable due to the manner in which shots for the 3-D VSP survey were undertaken and also due to the recording taking place only in one well location.

P-wave imaging

Two approaches were taken for the VSPCDP mapping of P-wave reflections (Figure 10). One approach was to use conventional raytracing and the other was to use amplitude semblance as discussed in Gulati et al. (1997). The elastic model used for the raytrace mappings is shown in Table 1.The model was interactively built until traveltimes computed by raytracing through the model matched with the observed traveltimes.

Figures 12 and 13 show an inline from the VSPCDP stacks using the two mapping methods. The two are remarkably similar except at bin locations further from the well where the raytracing method yields more coherent reflections. This is more due to an incomplete implementation than due to the traveltime moveout approximation of the latter method. Figure 14 shows the correlation between the two results.

The stacked sections were then trace equalized followed by time-variant spectral whitening. To interpret the stacked volumes using standard interpretive techniques, we would require that every bin location be represented by a reflectivity value. As this was not possible with the 3-D VSP survey at hand, f-xy deconvolution was then used to fill in empty bin locations. F-xy deconvolution also serves to increase the coherency of reflection events (compare Figures 12 and 15).

Contents

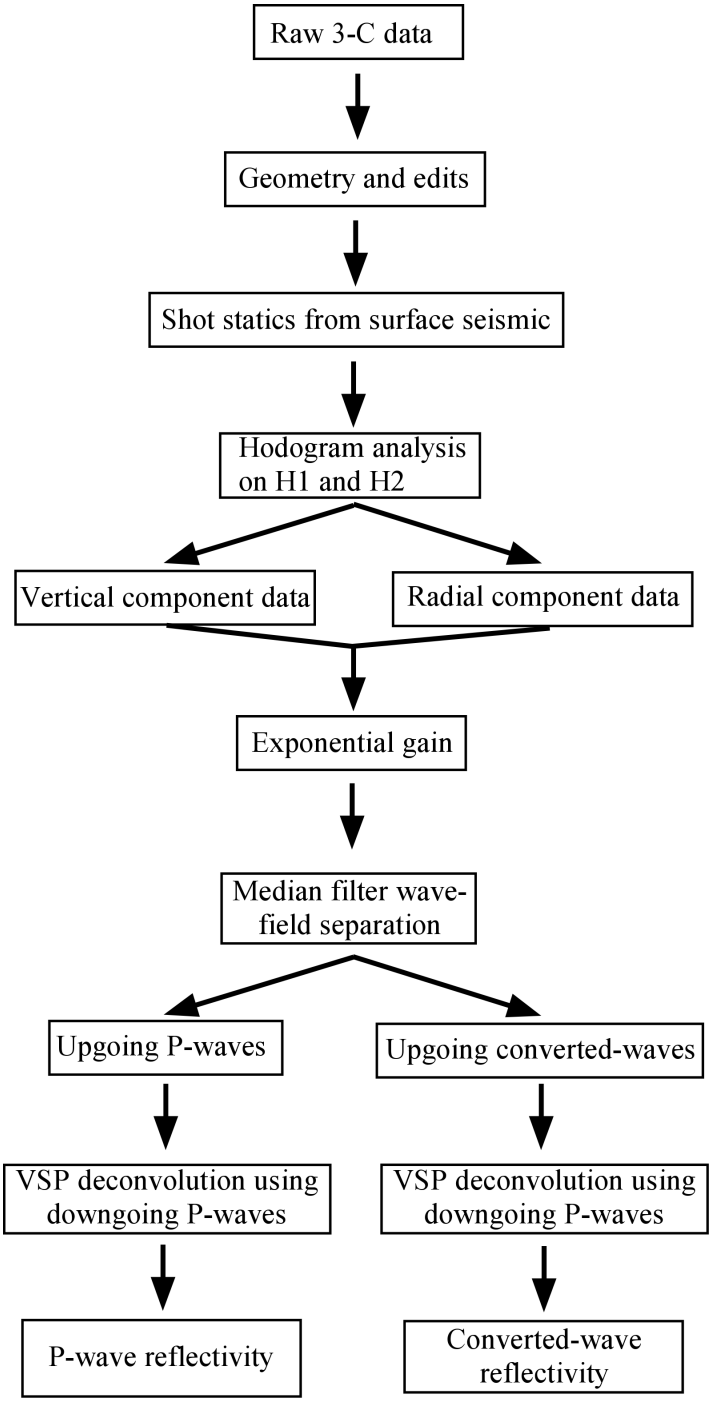

Fig.2. Processing flow to obtain deconvolved upgoing P-wave and converted-waves from the 3C-3D VSP data.

Contents

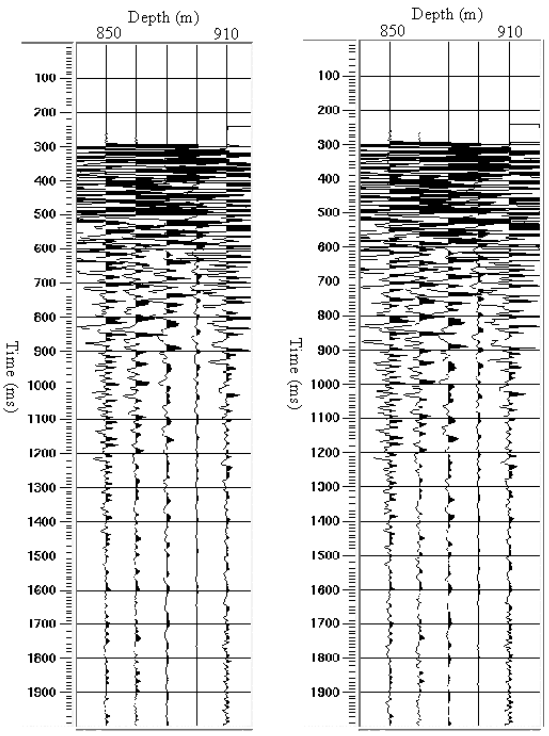

(a) Raw vertical component. (b) Raw H1 component.

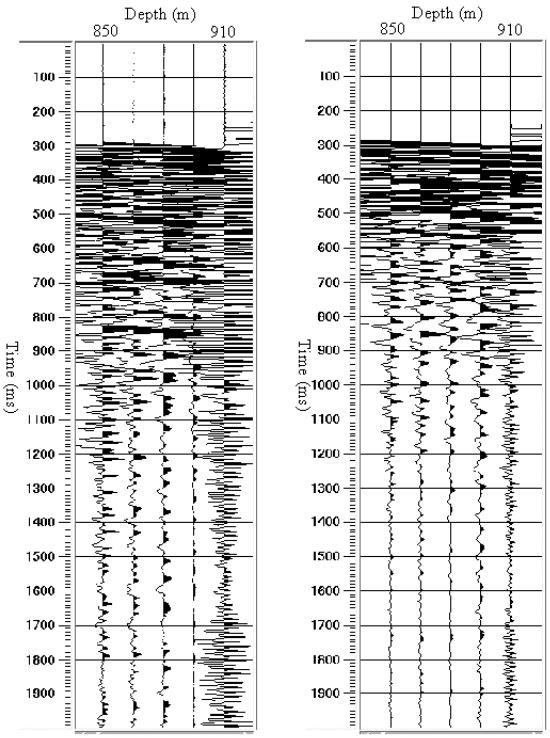

(c) Raw H2 component. (d) Radial component.

Contents

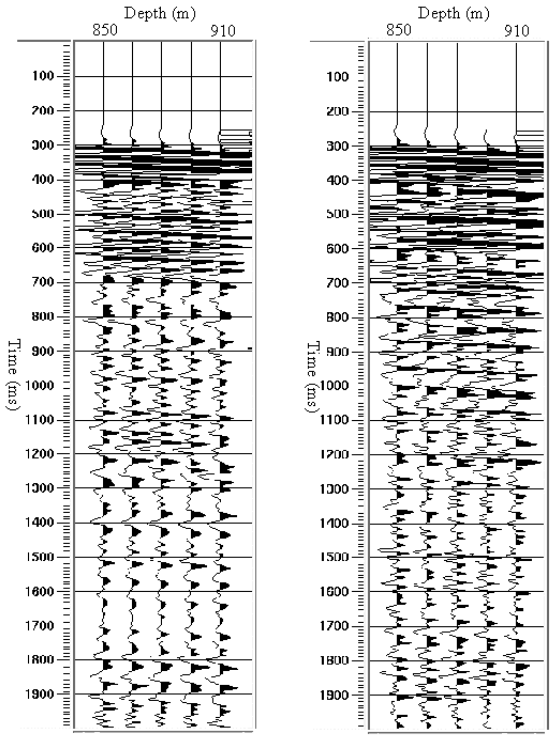

(e) Donwgoing P-waves. (f) Downgoing converted-waves.

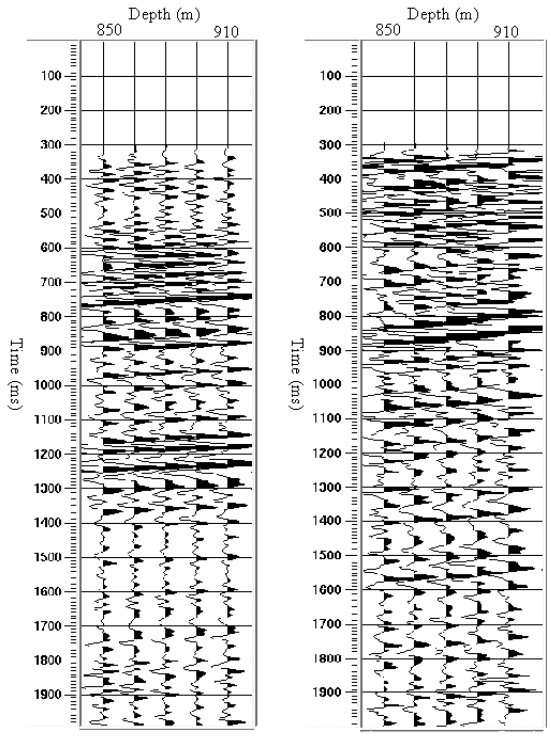

(f) Upgoing P-waves. (g) Upgoing converted-waves.

Fig.3. Shot gathers for shot at an offset of 372m from the well.

Contents

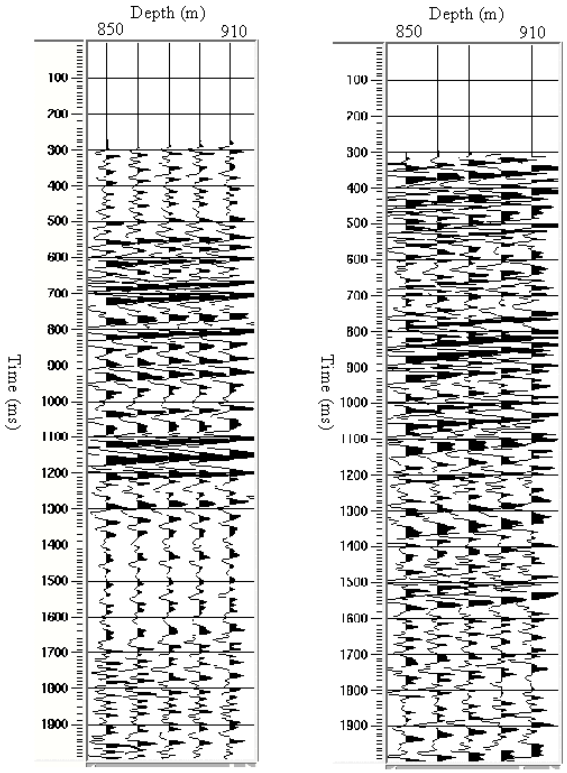

(a) Upgoing P-waves. (b) Upgoing converted-waves.

Fig.4. Deconvolved upgoing waves for the same shot gather as in Fig. 3.

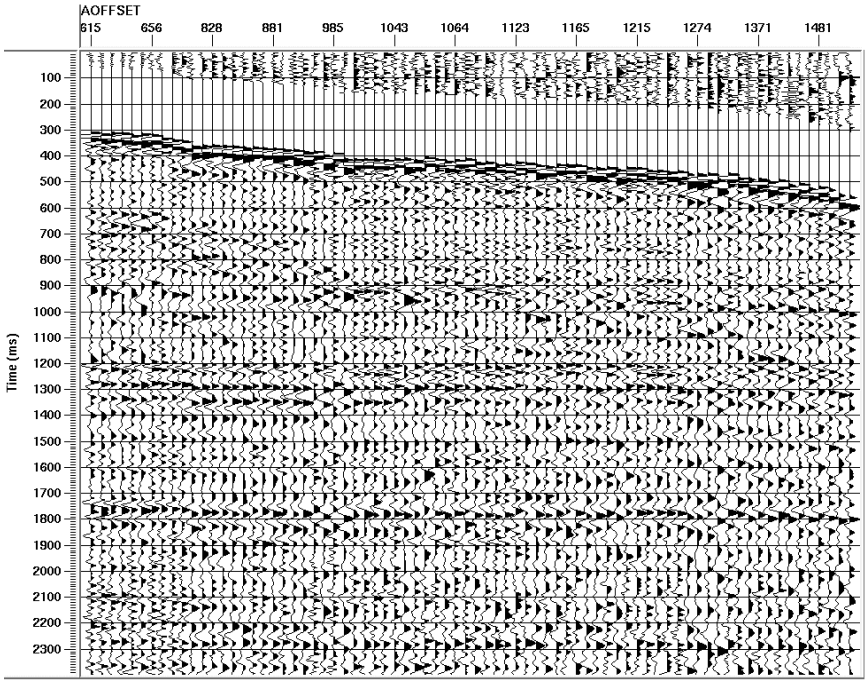

Fig.5. Raw vertical component receiver gather for receiver at depth 655m displayed with an AGC window of 500ms.

Contents

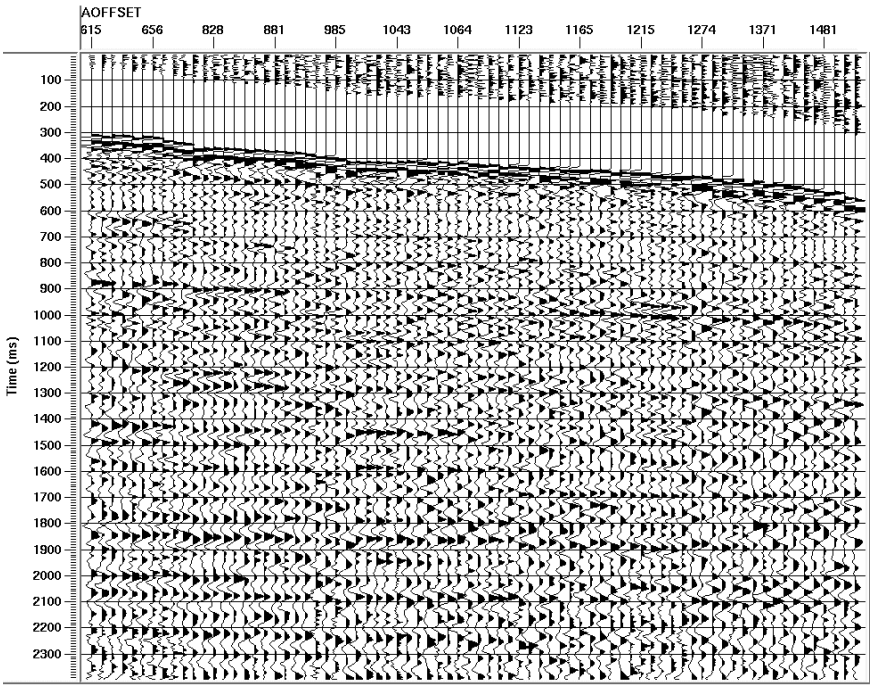

Fig.6. Raw H1 component receiver gather for receiver at depth 655m displayed with an AGC window of 500ms.

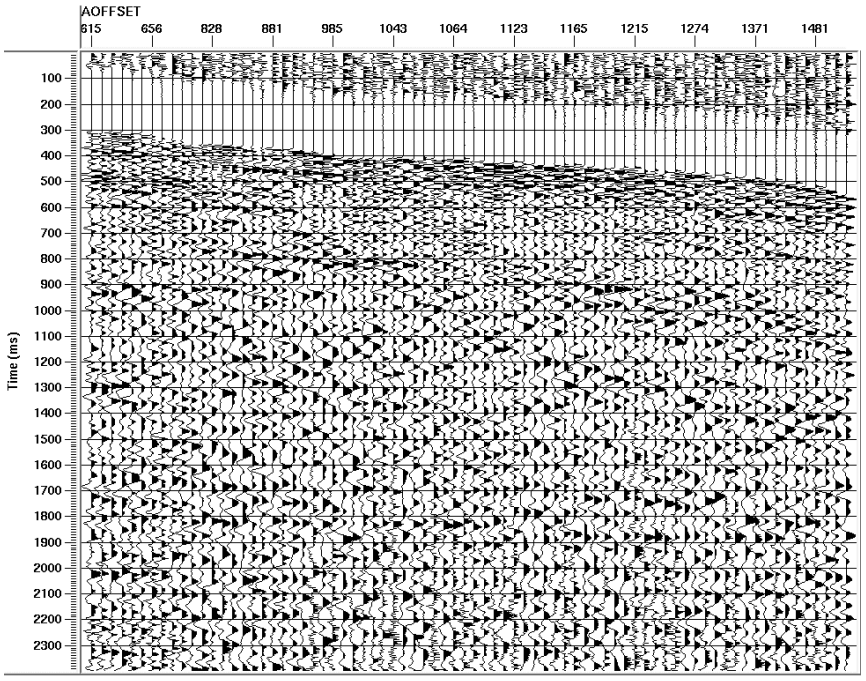

Fig.7. Raw H2 component receiver gather for receiver at depth 655m displayed with an AGC window of 500ms.

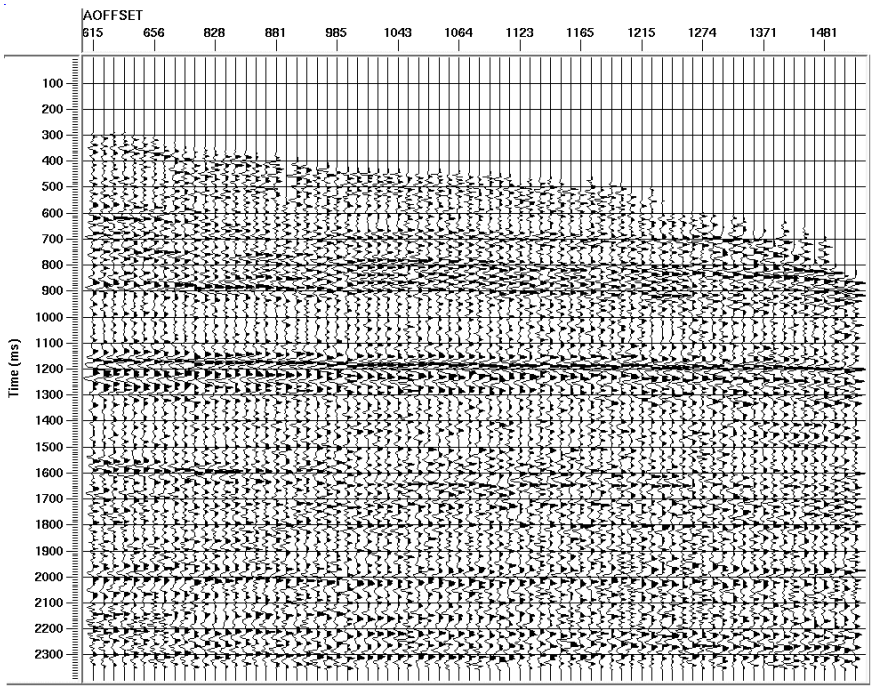

Fig.8. Deconvolved upgoing P-waves on vertical component receiver gather for receiver at depth 655m. Data is displayed with an AGC window of 500ms.

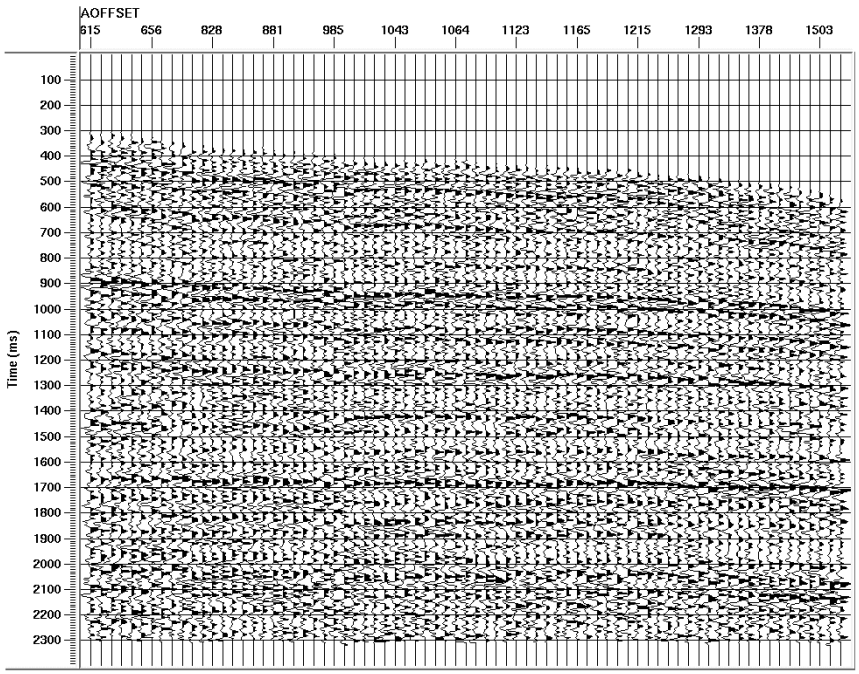

Fig.9. Deconvolved upgoing converted-waves on radial component receiver gather for receiver at depth 655m. Data is displayed with an AGC window of 500ms.

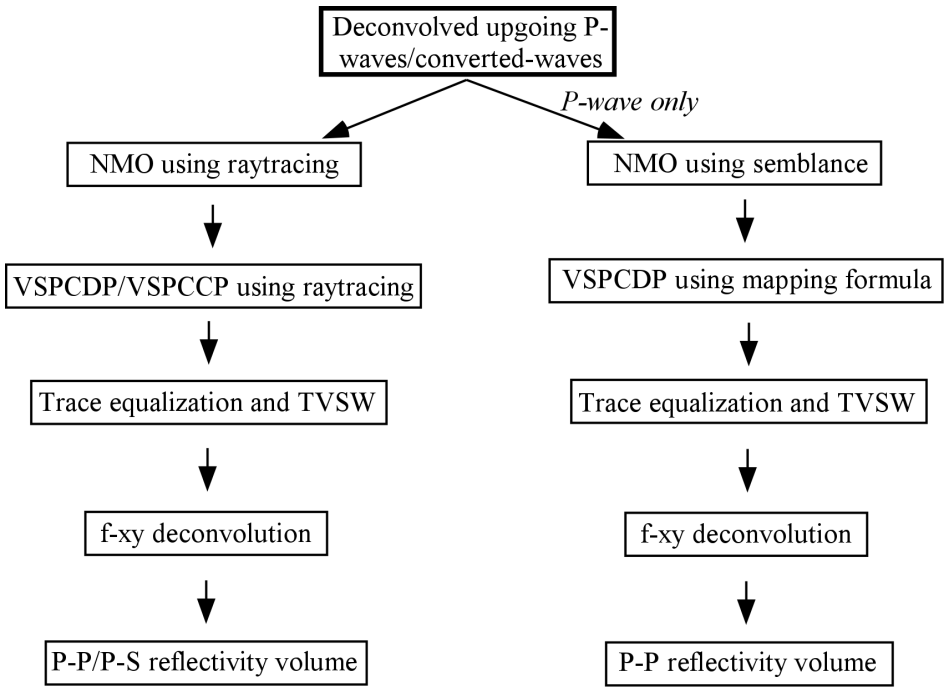

Fig.10. Flow for imaging the deconvolved upgoing P-wave and converted-wave reflections.

Table 1. Elastic model used for raytrace mapping. Datum depth = 1000m asl.

Depth below datum (m)	P-wave velocity (m/s)	S-wave velocity (m/s)
224	3000	1500
600	3050	1605
963	3275	1725
1231	3512	1975
1486	3672	2062
1600	4179	2347
1733	4179	3125
2000	5500	3425
2500	6000	3690
3000	5900	3650
3500	5850	3625
6500	5850	3650

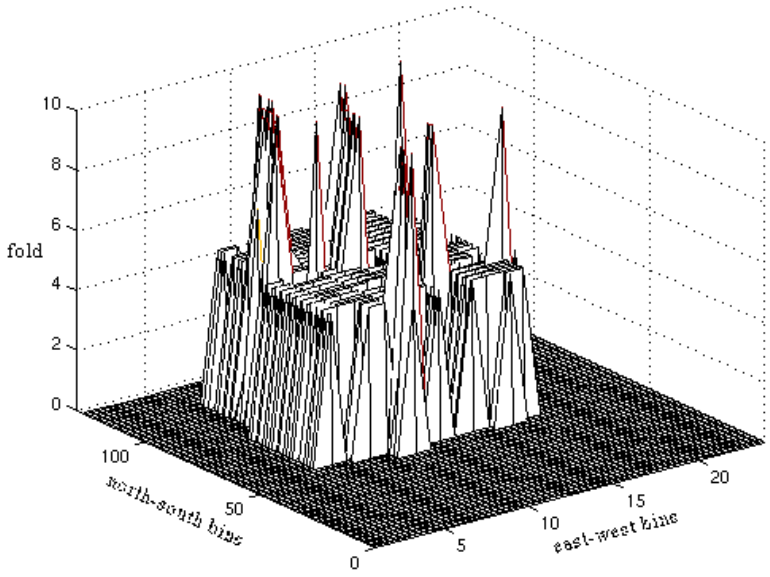

Fig.11. Fold distribution for P-P data at the target depth of 1500m when using a bin size of 110m by 20m.

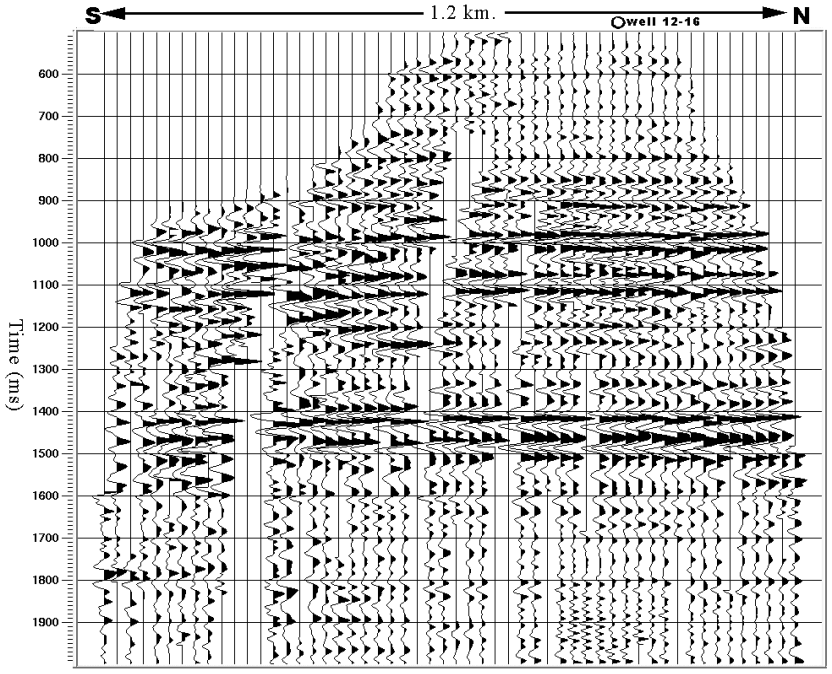

Fig.12. An inline section from the P-wave 3-D volume obtained from raytracing. Shown also is the crossline surface location of well 12-16.

Contents

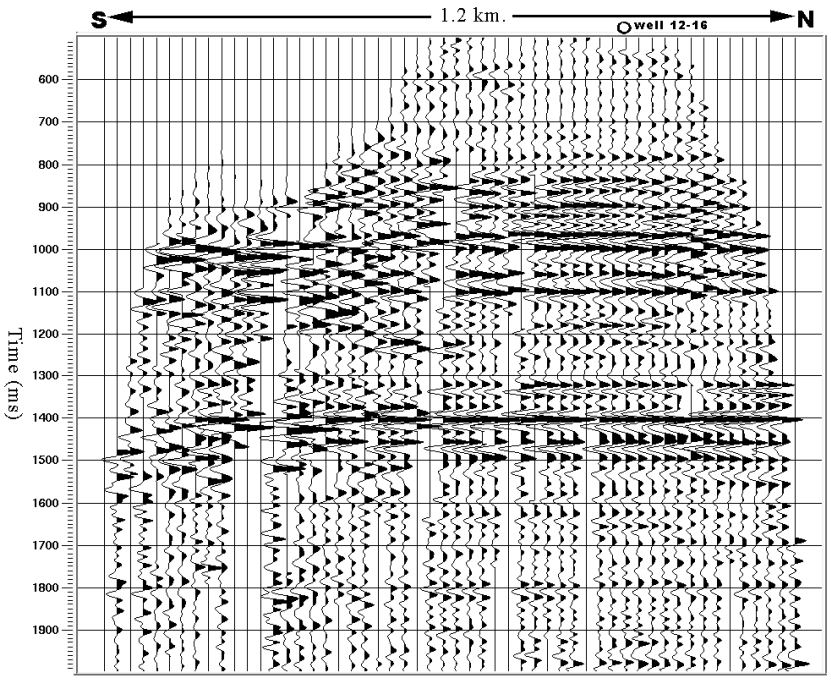

Fig.13. An inline section from the P-wave 3-D volume obtained from semblance and mapping formula. Shown also is the crossline surface location of well 12-16.

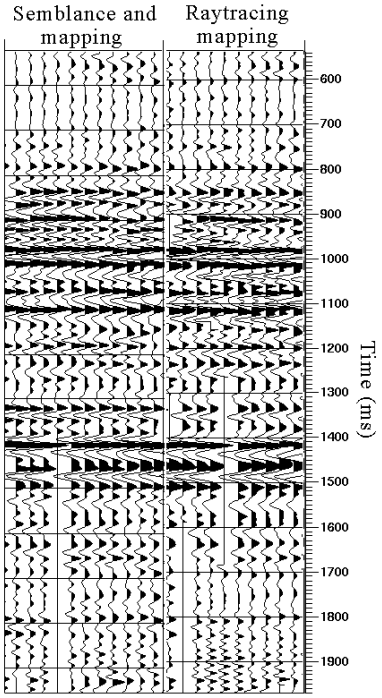

Fig.14. Correlation of the 3-D VSPCDP stacking of P-wave reflections using two different mapping methods.

Contents

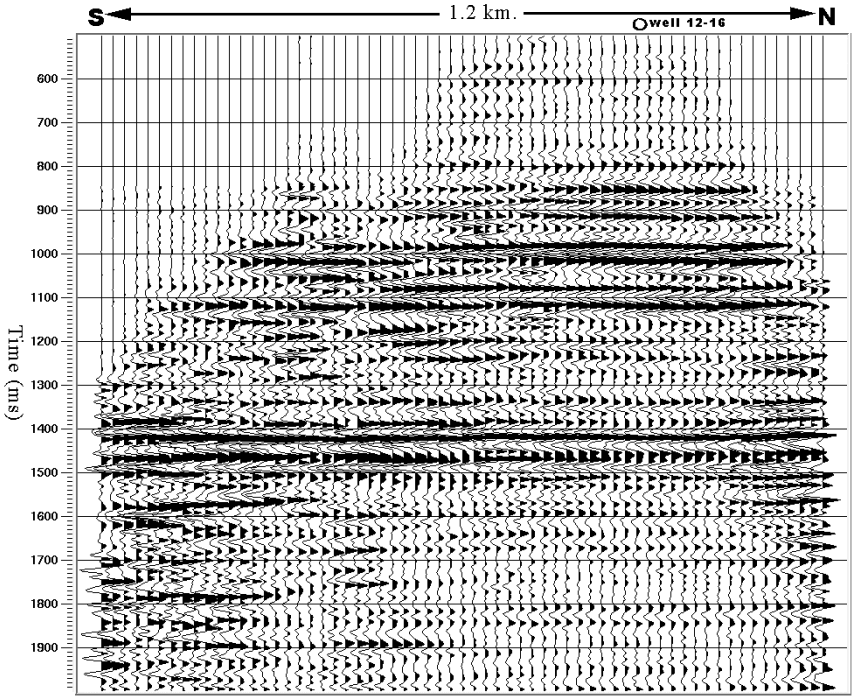

Fig.15. Same inline section as in Figure 12 but after trace equalization, time-variant spectral whitening and f-xy deconvolution.

Converted-wave imaging

The converted-wave reflection mapping was done using the conventional raytracing approach only. The radial component data was VSPCCP stacked using the same bin size of 110m by 20m as in the case of P-wave data (Figure 16). The stacked data was then passed through the same processes as in the case of P-wave data to give the final interpretable volume (Figure 17). Unlike P-wave data, all mode-converted events experience strong amplitude variation with offset and which is known to be a quasi-sinusoidal function of the incident angle (Gulati and Stewart, 1997). Likewise for the present survey, strong converted-waves are observed for shallow reflectors (Figures 16 and 17) as the P-wave incident angle for these appear to fall in the zone where mode-conversion is maximum. On the other hand, in the case of deeper converted-wave events such as the one at around 2100ms, the expected sinusoidal-like amplitude behaviour is visually evident. Thus, when designing a 3C-3D VSP survey for converted-wave interpretation, care should be taken to place the receivers at depths such that P-wave incident angles at the target depth fall in the range of maximum mode conversion. Fortunately, the present survey appears to satisfy this criterion for the target reflection time around 1550ms.

P-WAVE AND CONVERTED-WAVE CORRELATION AND INTERPRETATION

P-wave interpretation

Formation tops were identified on the 3-D VSP P-wave image by correlating it with images from a previously interpreted surface 3C-3D survey in the area (Figure 18). Overall, there exists good correlation between the two although the VSP is lower frequency. Following this correlation, a time slice at the channel level was obtained from the VSP. Figures 19 and 20 show the time slices for the VSP from the two mapping methods and Figure 21 shows the corresponding time slice from the surface 3-D survey. Both the time slices from the 3-D VSP show a similar northeast-southwest trend which is evident on the surface time slice as well.

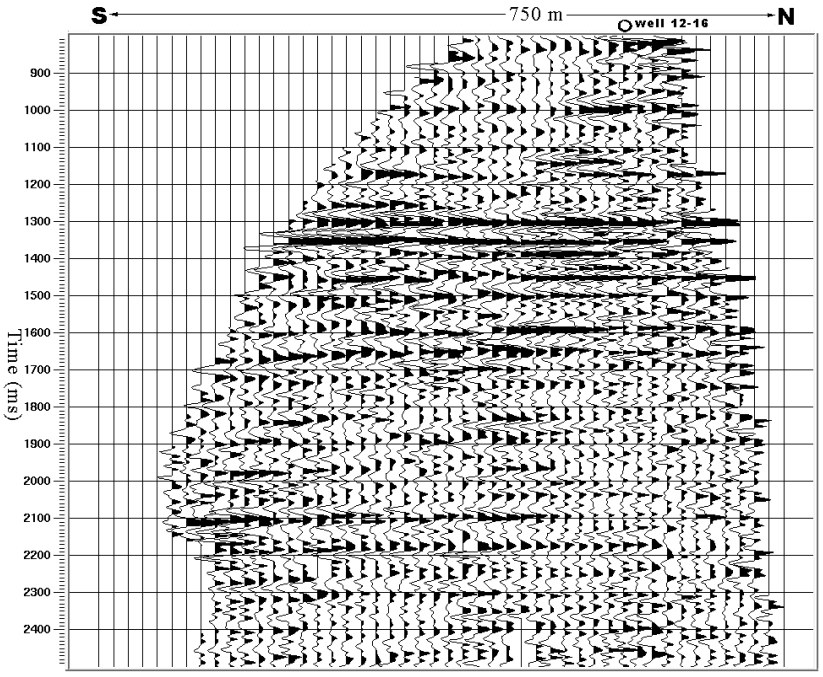

Fig.16. An inline section from the converted-wave 3-D volume obtained from raytracing. Shown also is the crossline surface location of well 12-16.

Contents

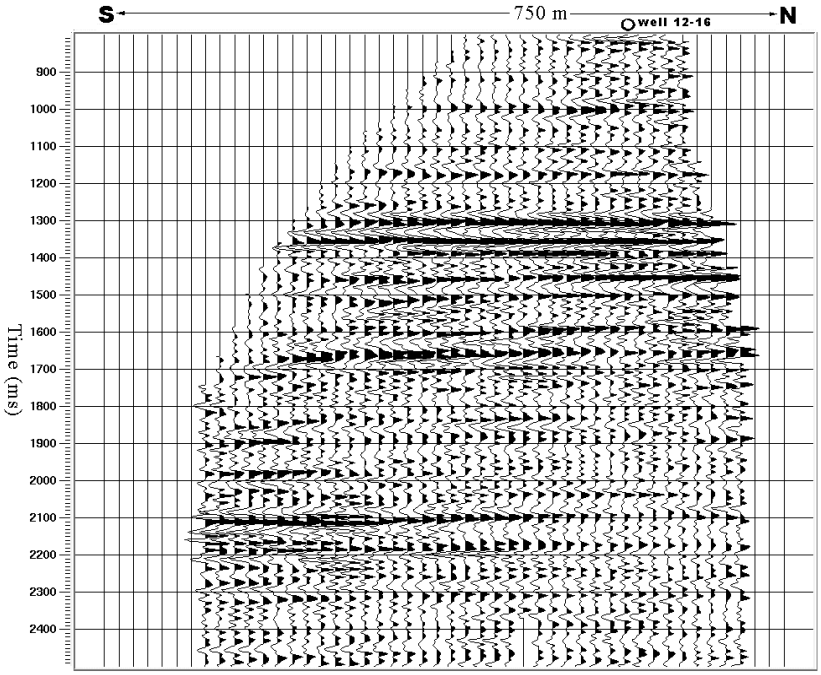

Fig.17. Same inline section as in Figure 16 but after trace equalization, time-variant spectral whitening and f-xy deconvolution.

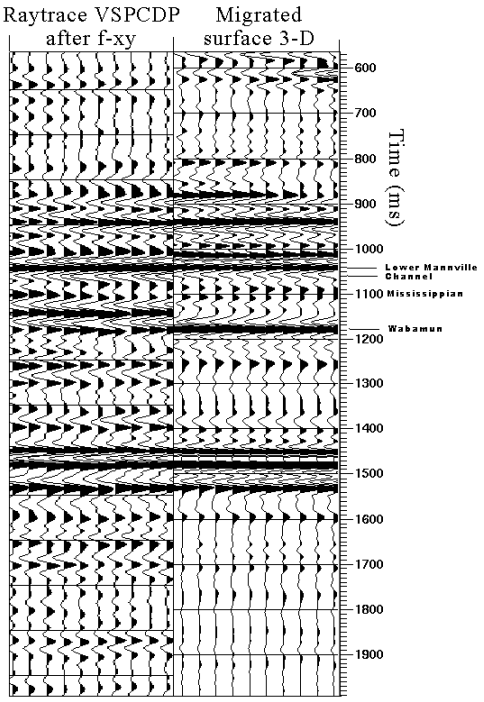

Fig.18. 3-D VSP P-wave correlation with migrated surface 3-D P-wave data. The VSP is displayed with reversed polarity.

Contents

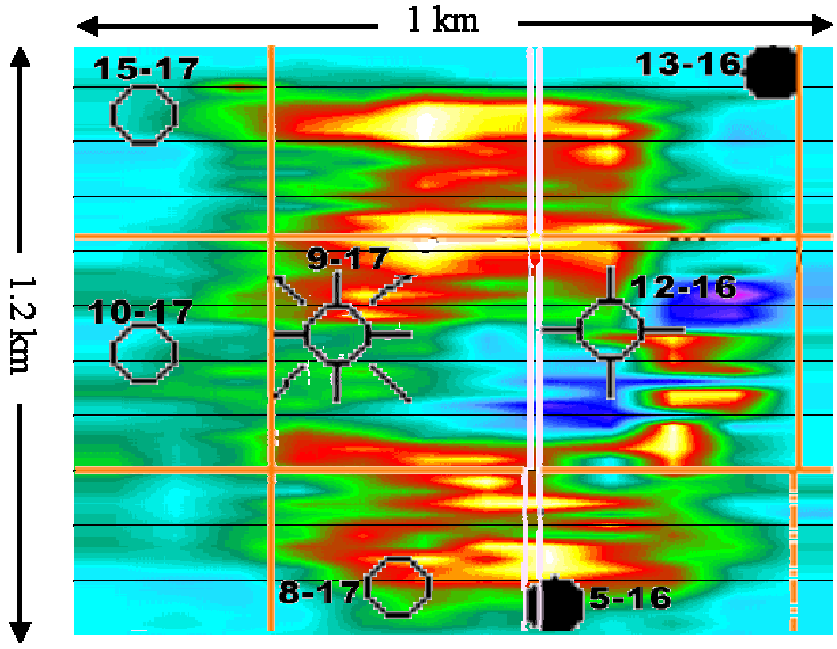

Fig.19. P-wave time slice at the channel level from the raytraced VSPCDP volume with flattening at the Mannville.

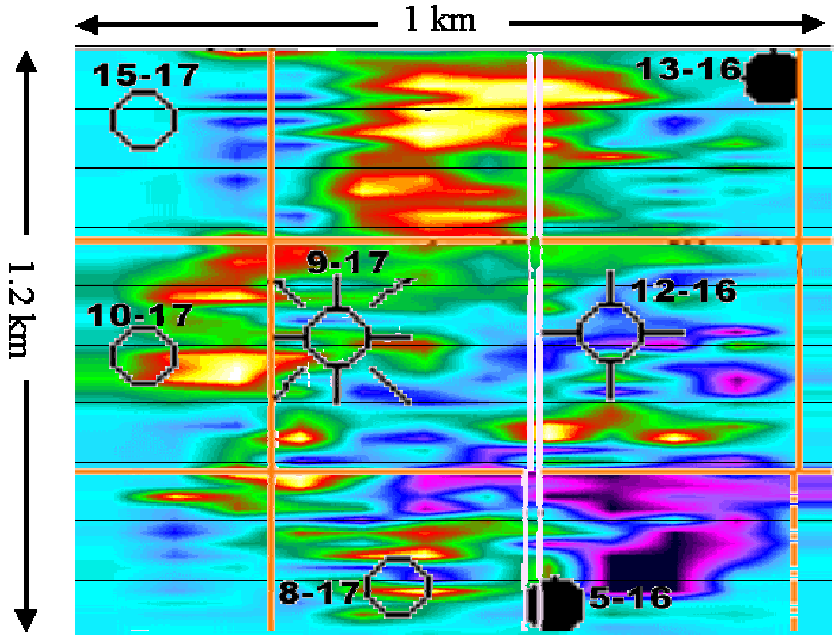

Fig.20. P-wave time slice at the channel level from the semblance and mapping formula VSPCDP volume with flattening at the Mannville.

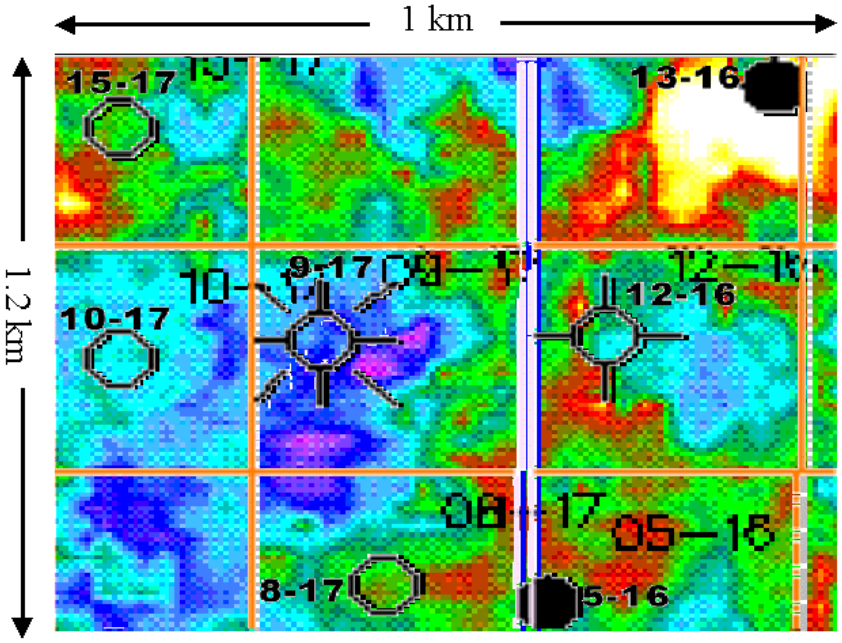

Fig.21. P-wave time slice at the channel level from the migrated surface 3-D volume with flattening at the Mannville (modified from Yang et al., 1996).

Figure 22 shows the entire time slice from the surface 3-D survey. It shows a north-south channel trend joined by another channel body from the west in the north-side of the map. Figure 23 shows the same time slice but with the time slice from the raytraced 3-D VSP inset into it. Comparing Figures 22 amd 23, one can observe that the channel trend is similar in both the time slices. However, the channel in the northern part of the map appears to have a more easterly trend in the original time slice of Figure 22.

Converted-wave interpretation

The converted-wave image from the VSP was also correlated and interpreted in a similar manner. Formation tops on the converted-wave data from the VSP were identified by correlating it with a previously interpreted surface 3C-3D image in the area (Figure 24). In the zone of interest, the converted-wave from the VSP appears to show somewhat better resolution than the converted-wave image from the surface seismic. However, at later times, the surface image is higher frequency compared to the VSP image.

In addition, the above converted-wave images were also correlated with P-wave images from the 3-D VSP and the surface 3-D, with images from an offset 3-C VSP and with synthetics derived from well-logs (Figure 25). From these correlations, the channel anomaly on the converted-wave 3-D VSP image is seen to be a trough. Following this, a time slice at the channel level was obtained for the converted-wave image from the 3-D VSP (Figure 26). The corresponding time slice from the surface 3C-3D survey is shown in Figure 27. Due to their small size, it is difficult to interpret these time slices. Figure 28 shows the converted-wave time slice from the entire 3C-3D survey and Figure 29 is the same time slice but with the converted-wave time

Contents

slice from the 3-D VSP inset into it. The north-south trending channel has a easterly drift in the north part of the map in Figure 28. The same trend is seen in Figure 29 as well but the drift to the east starts more to the south in Figure 29 than in Figure 28.

CONCLUSIONS

The Blackfoot 3-D VSP experiment has shown that acquisition of simultaneous 3-D VSP and surface seismic surveys is possible and is cost-effective. Basic processing of the 3-D VSP data has shown the robustness of such simultaneous acquisitions. There is also a need for improvement in the wavefield separation and deconvolution processes and new techniques need to be developed.

VSPCDP stacking of the 3-D VSP data using amplitude semblance analysis was observed to yield meaningful results. While the recording geometry for the 3-D VSP was not ideal, both P-wave and converted-wave VSP images were observed to correlate well with images from the surface 3C-3D in the same area. Time slices from the 3-D VSP also indicated the channel trend evident on the surface data. Results from this preliminary survey show the promise of the 3-D VSP. The 3-D VSP could be a significant tool to obtain high-resolution 3-D images near the borehole.

REFERENCES

Bicquart, P., 1998, Application of Kirchhoff migration to 3D-VSP: Presented at 68th Ann. Intl. SEG Mtg., Expand. Abst., 389-392.

Boelle, J., Kiaser, P. and Maocec, E., 1998, Difficulties and clues in 3D VSP processing: Presented at 68th Ann. Intl. SEG Mtg., Expand. Abst., 373-376.

Chang, W. and McMechan, G.A., 1986, Reverse-time migration of offset vertical seismic profiling data using he excitation-time imaging condition: Geophysics, 51, 67-84.

Chen, G., 1998, 3D VSP CDP mapping with interactive reflection traveltime display: Presented at 68th Ann. Intl. SEG Mtg., Expand. Abst., 361-364.

Chen, H. and McMechan, G.A., 1992, 3-D pre-stack depth migration for salt and sub-salt structures using reverse-VSP data: J. Seis. Explor., 281-291.

Chen, G. and Peron, J.F., 1998, Mapping of 3D VSP data using quick ray tracing: Presented at 68th Ann. Intl. SEG Mtg., Expand. Abst., 365-368.

Clochard, V., Compte, P., Nicoletis, L., Lucas-Svay, J. and Dillon, P.B., 1997, 3D walk-away imaging in the overthrust model: Presented at the 57th Ann. EAGE Mtg., E047.

Clochard, V., Nicoletis, L., Svay-Lucas, J., Mendes, M. and Anjos, L., 1998, 3-C imaging of 3D walk-away data in regard to preprocessing: Presented at 68th Ann. Intl. SEG Mtg., Expand. Abst., 377-380.

Dangerfield, 1996, Shallow 3-D seismic and a 3-D borehole profile at Ekofisk field, in Ed. Brown, A., *Interpretation of three-dimensional seismic data*, AAPG Memoir 42.

Esmersoy, C., 1990, Inversion of P and SV waves from multicomponent offset vertical seismic profiles: Geophysics, 55, 39-50.

Fairborn, J.W. and Harding, R.S., Jr., 1996, 3D seismic velocity tomography at SPR sinkhole site, Weeks Island, Louisiana: Presented at 59th Ann. Intl. SEG Mtg., Expand. Abst., 896-898.

Farmer, P., Chapman, C., Fryer, A., Paul, A. and Sandvin, O., 1997, 3-D tomographic inversion and depth migration of VSP data. Presented at 60th Ann. Intl. SEG Mtg., Expand. Abst.

First Break, 1997, Large 3D VSP survey completed on BP Magnus field: First Break, 15, 290.

Gulati, J.S. and Stewart, R.R., 1997, Seismic exploration through high-velocity layers: Presented at 67th Ann. Intl. SEG Mtg., Expand. Abst., 1297-1300.

Gulati, J.S., Stewart, R.R., Peron, J.F., and Parkin, J.M.1997, 3C-3D VSP: Normal moveout correction and VSPCDP transformation, CREWES Research Report, Chpt. 7.

Hoffe, B.H., Stewart, R.R., Bland, H.C., Gallant, E.V., and Bertram, M.B., 1998, The Blackfoot high-resolution 3-C seismic survey: design and initial results, Presented at 68th Ann. Intl. SEG Mtg., Expand. Abst., 103-106.

Kennett, P., Ireson, R.L., and Conn, P.J., 1980, Vertical seismic profiles: Their applications in exploration geophysics: Geophysical Prospecting, 28, 676-699.

Labonte, S., 1990, Modal separation, mapping, and inverting three-component VSP data: M.Sc. Thesis, The University of Calgary.

Margrave, G.F., Lawton, D.C., and Stewart, R.R., 1998, Interpreting channel sands with 3C-3D seismic data: The Leading Edge, 4, 509-513.

Miller, S.L.M., 1996, Multicomponent seismic data interpretation: M.Sc. thesis, University of Calgary.

Mittet, R., Landro, M., Hokstad, K. and Ostmo, S., 1997, A methodology for 3D elastic depth imaging of marine 3D walkaway data. Presented at the 57th Ann. EAGE Mtg., E046.

Shekhtman, G.A. Zernov, A.E., Potapov, O.A., Lebedeva, I.I., Sokolova, K.B., 1993, Areal modification of the VSP method: Presented at the 55th Ann. EAGE. Mtg., P090.

Stewart, R.R. and Zhang, Q., 1996, 2-D and 3-D VSP interpretation: Blackfoot field, Alberta, CREWES Research Report, Chpt. 41.

Stewart, R.R. and Gulati, J.S., 1997, 3-D VSP: Recent history and future promise, CREWES Research Report, Chpt. 9.

Sun, Z. and Stewart, R.R., 1994, 3-D reverse VSP: CREWES Research Report, v. 6,Chpt. 12.

Van der Pal, R.C., Bacon, M. and Pronk, D., 1996, 3D walkaway VSP, enhancing seismic resolution for development optimization of the Brent field: First Break, 14, 463-469.

Whitmore, D.N., and Lines, L.R., 1986, Vertical seismic profiling depth migration: Geophysics, 51, 1087-1109.

Wood, J.M., and Hopkins, J.C., 1992, Traps associated with paleovalleys and interfluves in uncorfomity bounded sequence: Lower Cretaceous Glauconitic Member, Southern Alberta, Canada: AAPG Bull., 76(6), 904-926.

Wyatt, K.D. and Wyatt, S.B., 1984, Determining subsurface structure using the vertical seismic profile, in Eds. Toksoz, N.M. and Stewart, R.R., *Vertical Seismic Profiling, Part B-Advanced Concepts*, Geophys. Press.

Yang, G.Y.C., Lawton, D.C., Stewart, R.R., Miller, S.L.M., Potter, C.C., and Simin, V., 1996, Interpretation and analysis of the Blackfoot 3C-3D survey, CREWES Project Research Report, Chpt. 46.

Zhang, Q., Stewart R.R., and Sun, Z., 1995, 3-D VSP: Survey design and processing: CREWES Project Research Report, v. 7, ch. 34, 1-24.

Zhang, Q., Stewart R.R. and Sun, Z., 1997, 3D borehole seismic imaging and correlation – a field experiment. Presented at the 59th Ann. EAGE Mtg., E048.

Zhang, Q., Stewart R.R., Parkin, J.M. and Sun, Z., 1996, Analysis of the Blackfoot 3C-3D VSP survey, CREWES Project Research Report, Chpt. 40.

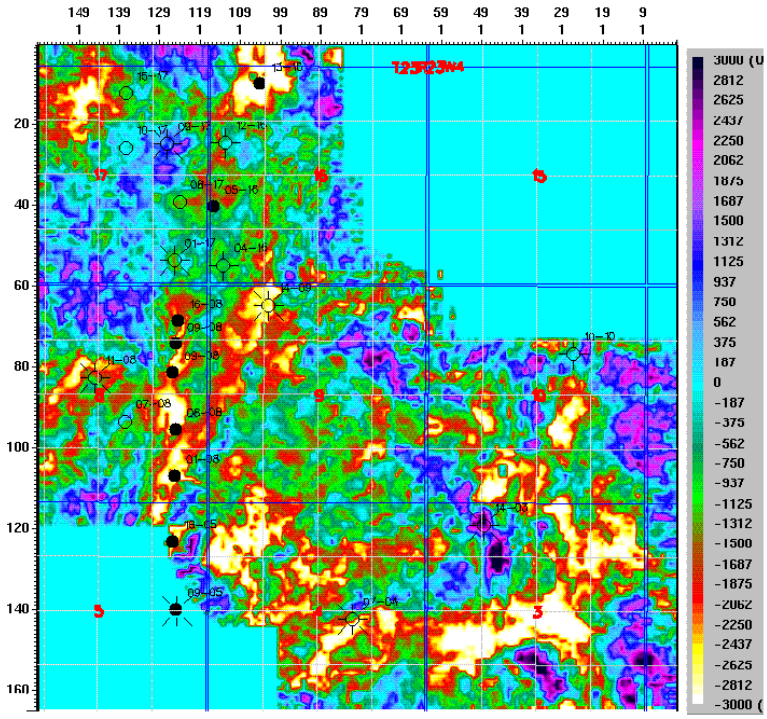

Fig.22. P-wave time slice at the channel level for the entire surface 3-D survey (from Yang et al., 1996).

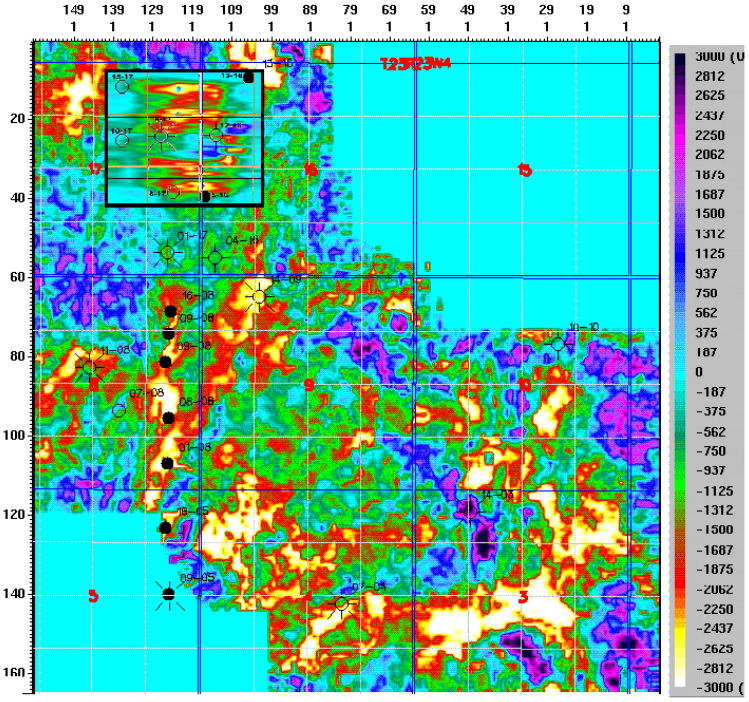

Fig.23. P-wave time slice at the channel level from Figure 17 inset into the corresponding time slice for the entire 3-D survey.

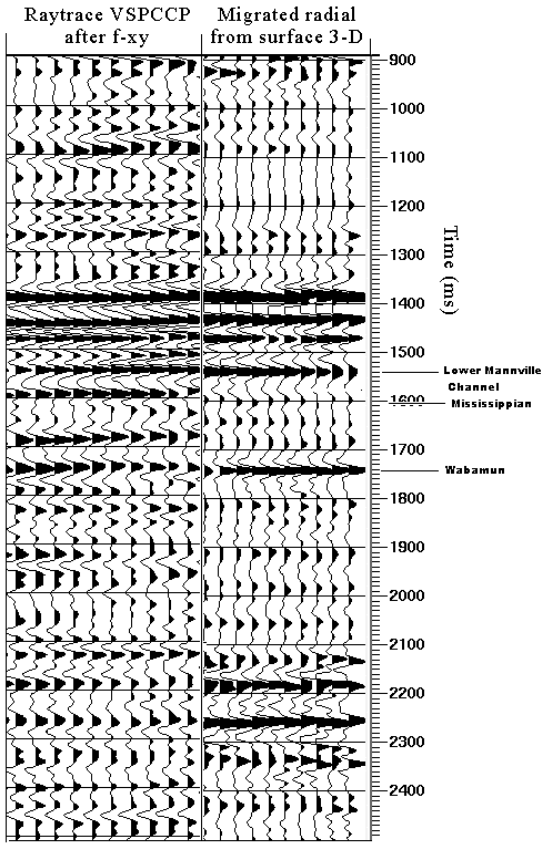

Fig.24. 3-D VSP converted-wave correlation with migrated 3-D converted-wave data from surface seismic.

Contents

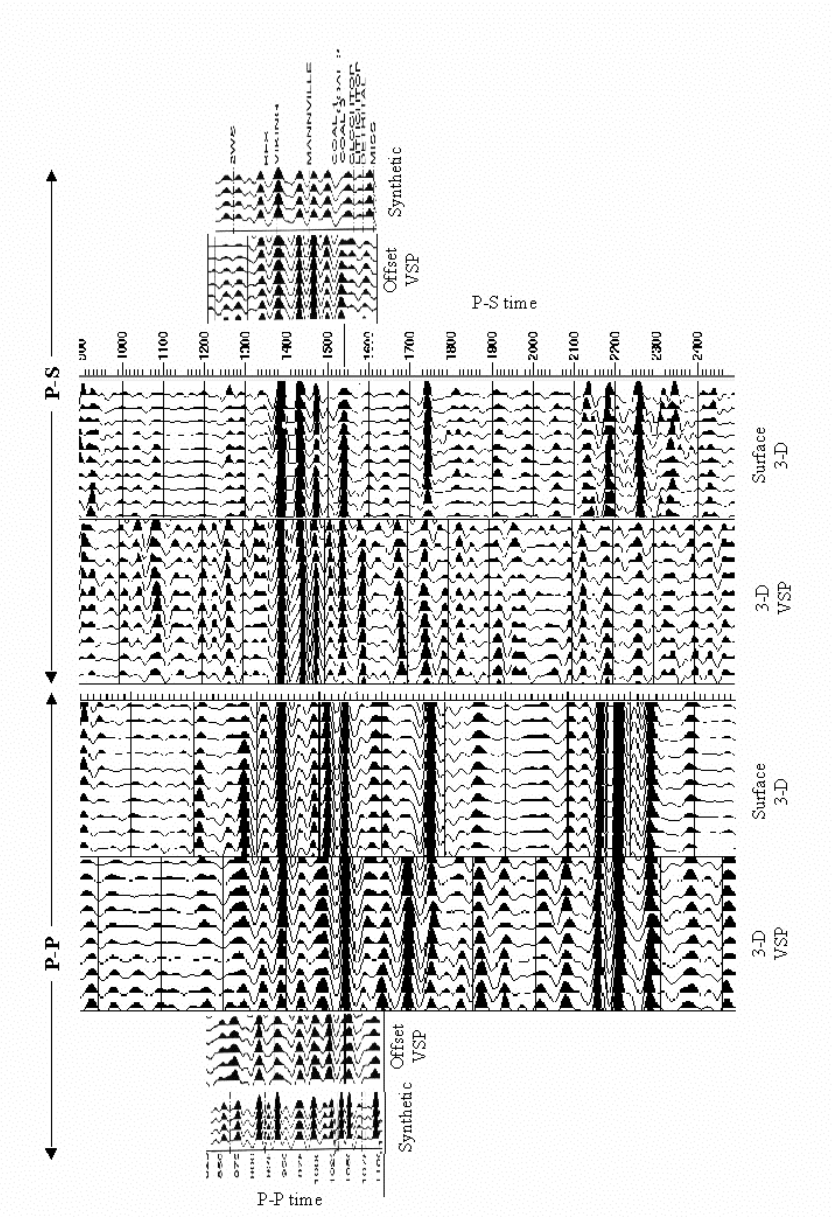

Fig. 25. Correlations between synthetics and different data

Contents

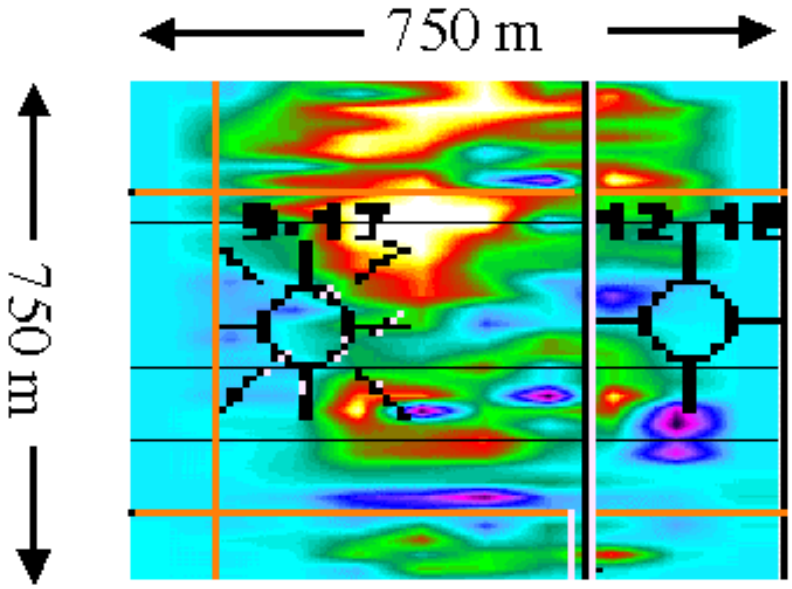

Fig.26. Converted-wave time slice at the channel level, flattened at the Mannville, from the 3-D VSP.

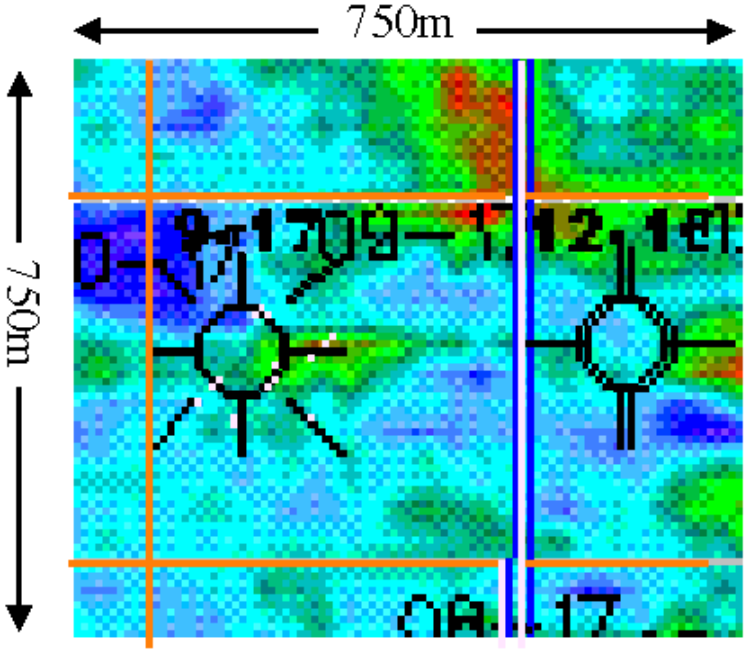

Fig.27. Converted-wave time slice at the channel level, flattened at the Mannville, for the area in Figure 22 from the migrated surface 3-D radial data (modified from Yang et al., 1996).

Contents

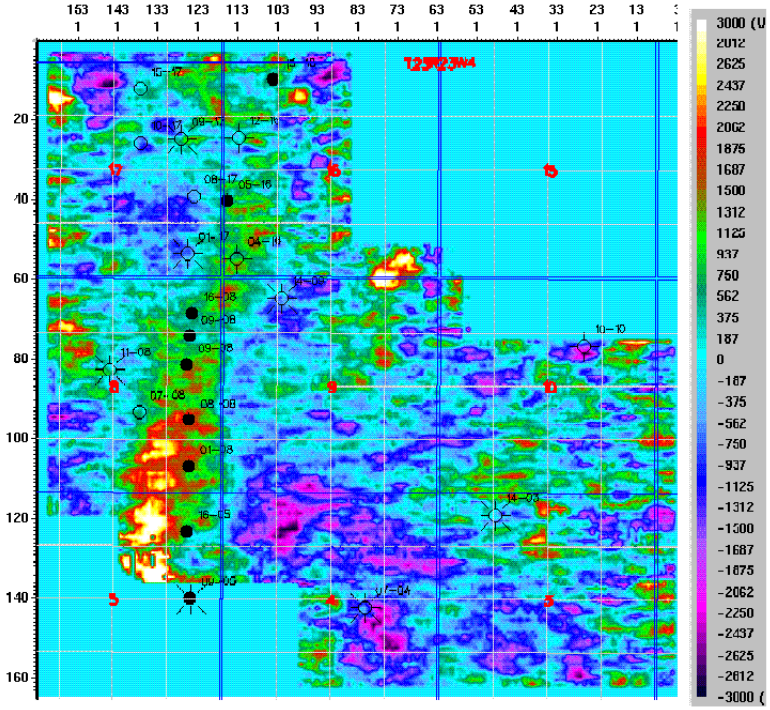

Fig.28. Converted-wave time slice at the channel level from the migrated surface 3-D radial data (from Yang et al., 1996).

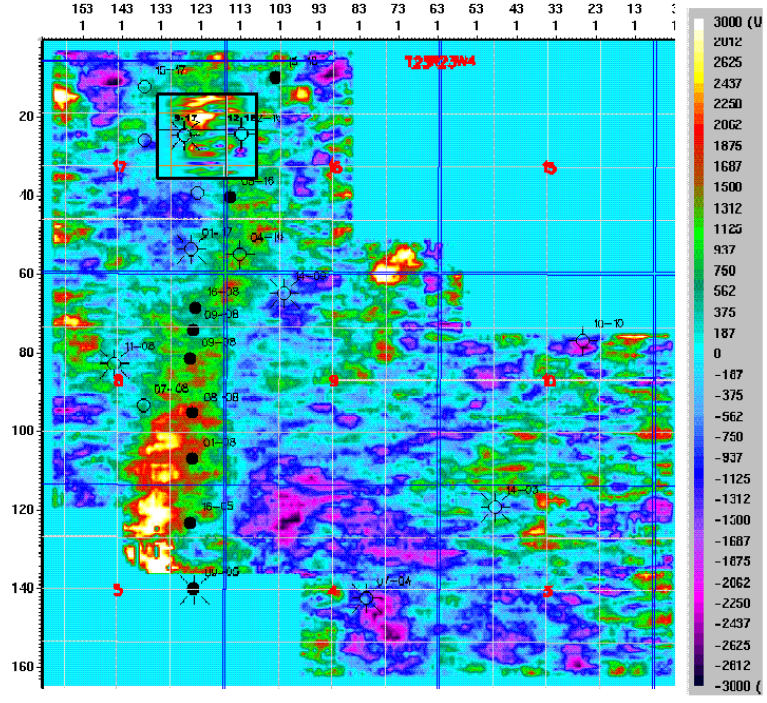

Fig.29. Converted-wave time slice at the channel level from Figure 22 inset into the corresponding time slice for the entire 3-D survey.

Contents